Acta Crystallographica Section D
Biological Crystallography
ISSN 0907-4449

Structural basis for non-catalytic and catalytic activities of ribonuclease III

Xinhua Ji

Macromolecular Crystallography Laboratory, National Cancer Institute, National Institutes of Health, Frederick, MD 21702, USA

Correspondence e-mail: jix@ncifcrf.gov

Received 31 January 2006
Accepted 29 March 2006

Ribonuclease III (RNase III) represents a highly conserved family of double-stranded (ds) RNA-specific endoribonucleases, exemplified by bacterial RNase III and eukaryotic Rnt1p, Drosha and Dicer. Bacterial RNase III, containing an endonuclease domain followed by a dsRNA-binding domain, is the most extensively studied member of the family. It can affect RNA structure and gene expression in either of two ways: as a processing enzyme that cleaves dsRNA or as a binding protein that binds but does not cleave dsRNA. The available biochemical and structural data support the existence of two distinct forms of the RNase III–dsRNA complex which reflect the dual activities of the protein. The information revealed by the structures of bacterial RNase III provides insight into the mechanism of dsRNA processing by all members of the family.

1. Introduction

Ribonuclease III (RNase III) represents a highly conserved family of double-stranded (ds) RNA-specific endoribonucleases (Robertson *et al.*, 1968; Court, 1993; Nicholson, 1996; Krainer, 1997; Nicholson, 1999; Filippov *et al.*, 2000). It plays important roles in dsRNA processing (Robertson *et al.*, 1968) and post-transcriptional gene-expression control (Court, 1993; Krainer, 1997; Wu *et al.*, 2000). RNase III has gained added importance with the recent discovery of the role that Dicer plays in RNA interference, a broad class of gene-silencing phenomena initiated by dsRNA (Bernstein *et al.*, 2001; Carthew, 2001). The RNase III family can be divided into four classes with increasing molecular weight and complexity of the polypeptide chain, including bacterial RNase III and eukaryotic Rnt1p, Drosha and Dicer (Fig. 1*a*). While Dicer, which produces small interfering RNAs, is currently the focus of intense interest, bacterial RNase IIIs such as *Escherichia coli* (Ec-RNase III) and *Aquifex aeolicus* RNase III (Aa-RNase III) serve as a paradigm for the entire family because they are structurally simpler, containing only two domains: an endonuclease domain (endoND) followed by a dsRNA-binding domain (dsRBD). In Aa-RNase III, the endoND contains 144 amino-acid residues and the dsRBD contains 70 amino-acid residues; there is a seven-residue linker between the two domains. Although the length of the endoND sequence varies between species (Fig. 1*a*), every endoND is characterized by a stretch of conserved residues which is known as the RNase III signature motif (Fig. 1*b*). A structure-based multiple sequence alignment of bacterial RNase III proteins can be found in Blaszczyk *et al.* (2004). It is the signature motif that led to the discovery of most members of the RNase III family.

Table 1
Three-dimensional structures of bacterial RNase III proteins.

Source	Protein	Mutation	Ligands	Resolution† (Å)	PDB code (reference)
E. coli	dsRBD			NMR	‡ (Kharrat *et al.*, 1995)
T. maritima	RNase III			2.00	1o0w§
M. tuberculosis	endoND¶		Ca^{2+}	2.10	2a11 (Akey & Berger, 2005)
A. aeolicus	endoND			2.15	1i4s (Blaszczyk *et al.*, 2001)
	endoND		Mn^{2+}	2.15	1jfz (Blaszczyk *et al.*, 2001)
	endoND		Mg^{2+}	2.30	1rc5 (Blaszczyk *et al.*, 2004)
	RNase III	E110K	dsRNA††	2.15	1rc7 (Blaszczyk *et al.*, 2004)
	RNase III		dsRNA‡‡	2.50	1yyk (Gan *et al.*, 2005)
	RNase III	E110K	dsRNA‡‡	2.90	1yyo (Gan *et al.*, 2005)
	RNase III		dsRNA§§	2.80	1yyw (Gan *et al.*, 2005)
	RNase III	E110Q	dsRNA¶¶	2.10	1yy9 (Gan *et al.*, 2005)
	RNase III	D44N	Mg^{2+}, dsRNA†††	2.05	2ez6 (Gan *et al.*, 2006)

† For crystal structures only. ‡ Coordinates are not available. § Primary reference is not available. ¶ Although the full-length Mt-RNase III was crystallized, the dsRBD was totally disordered and therefore not observed (see text for details). †† dsRNA formed by self-complementary sequence 5′-GGCGCGCGCC-3′. ‡‡ dsRNA formed by self-complementary sequence 5′-CGCGAAUUCGCG-3′. §§ dsRNA formed by self-complementary sequence 5′-AAAUAUAUAUUU-3′. ¶¶ dsRNA formed by self-complementary sequence 5′-CGAACUUCGCG-3′. ††† Product of a dsRNA-cleavage reaction, a dsRNA-like hairpin of sequence 5′-AAAGGUCAUUCGCAAGA-GUGGCCUUUAU-3′.

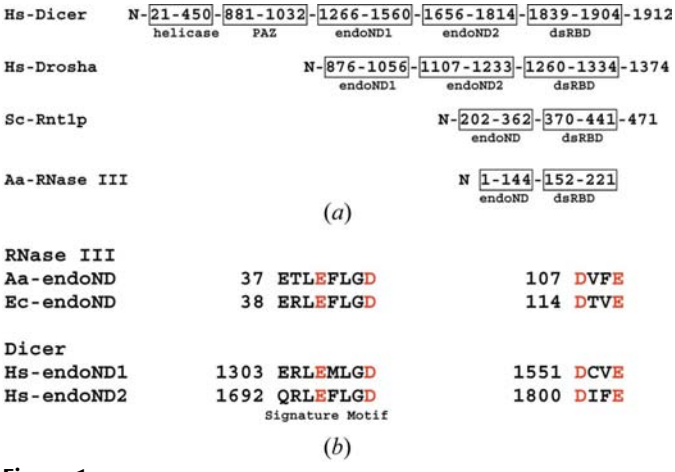

Figure 1
The RNase III family and catalytic residues. (*a*) Representatives of RNase III proteins: *Homo sapiens* Dicer (Hs-Dicer, SWISS-PROT Q9UPY3), *H. sapiens* Drosha (Hs-Drosha, SWISS-PROT Q9NRR4), *Saccharomyces cerevisiae* Rnt1p (Sc-Rnt1p, SWISS-PROT Q02555) and *A. aeolicus* RNase III (Aa-RNase III, SWISS-PROT O67082). Domain boundaries are indicated with boxed ranges of amino-acid sequence. (*b*) Signature motif in the endoND and the four catalytic residues of Aa-RNase III, Ec-RNase III (SWISS-PROT P0A7Y0) and Hs-Dicer. Note that the catalytic residues Glu40 and Asp44 are located in the signature motif.

Ec-RNase III, discovered in 1968 (Robertson *et al.*, 1968), is the most extensively studied member of the family. It can affect gene expression in either of two ways: as a processing enzyme or as a binding protein. As a processing enzyme, RNase III cleaves both natural and synthetic dsRNA into small duplex products averaging 10–18 base pairs in length (Robertson & Dunn, 1975; Dunn, 1982; Robertson, 1982; Court, 1993; Nicholson, 1999, 2003). As a binding protein, RNase III binds and stabilizes certain RNAs, thus suppressing the expression of certain genes (Guarneros, 1988; Court, 1993; Oppenheim *et al.*, 1993; Dasgupta *et al.*, 1998; Calin-Jageman & Nicholson, 2003). Two distinct functional forms of RNase III–dsRNA complex were hypothesized to reflect the dual activities of bacterial RNase III (Blaszczyk *et al.*, 2004).

The mechanisms of substrate recognition and cleavage by RNase III proteins provided by studies on the *E. coli* enzyme have demonstrated that a divalent metal ion is required for catalysis: Mg^{2+} is most likely to be the physiologically relevant species (Robertson *et al.*, 1968; Dunn, 1976; Li *et al.*, 1993), while Mn^{2+}, Co^{2+} and Ni^{2+} also support catalysis, but Ca^{2+}, Zn^{2+} and Sr^{2+} are inactive (Li *et al.*, 1993; Amarasinghe *et al.*, 2001; Campbell *et al.*, 2002).

2. Structures of RNase III proteins

To date, 12 three-dimensional structures of bacterial RNase III in various forms have been reported, of which 11 are available to the public (Table 1). Although the *E. coli* enzyme is the most extensively studied member of the RNase III family, structural information for RNase III has thus far been restricted to enzymes from other organisms, in particular that from *A. aeolicus* (Table 1). Therefore, the amino-acid residue numbers of Aa-RNase III will be used in the following sections unless otherwise stated. Known structures will be cited with their PDB codes whenever applicable.

2.1. The endoND: dimerization, catalytic valley and RNA-cleavage sites

The endoND is strictly conserved in all members of the RNase III family. In all available structures (Table 1), two endoNDs form a tight dimer (Fig. 2). The subunit interface in the endoND dimer is a hydrophobic surface. A total of 128 hydrophobic interactions (<4.0 Å) are found between the two subunits in the endoND dimer of Aa-RNase III, whereas only 20 hydrogen bonds/salt bridges exist at the subunit interface (Blaszczyk *et al.*, 2001). Identical 'ball-and-socket' junctions are formed at each end of the interface (Blaszczyk *et al.*, 2001). The 'ball' is the side chain of Phe41, located in the middle of the signature motif (Fig. 1*b*) in one endoND, while the 'socket' is a cavity in the partner endoND (Fig. 2). To assess the importance of this ball-and-socket interaction, residue Phe41 (Phe40 in Ec-RNase III) was mutated into Gly, Asp, Arg, Met and Trp and tested in the λ*N-lacZ* assay (Kameyama *et al.*, 1991; Dasgupta *et al.*, 1998) for RNase III activity (Blaszczyk *et al.*, 2001). The Gly, Asp and Arg substitutions gave rise to a defective enzyme, whereas the Met and Trp mutants were functional in the assay. It appears that the hydrophobic side chains of the latter mutants can still function as the ball in the ball-and-socket junction, but this interaction is precluded by charged side chains (F40D and F40R) or the absence of any side chain in this position (F40G). Dicer contains two endoNDs (Fig. 1*a*) which dimerize intramolecularly (Zhang *et*

al., 2004; MacRae *et al.*, 2006). Interestingly, in the first signature motif of human Dicer, a Met is located in the position of the ball residue (Fig. 1*b*).

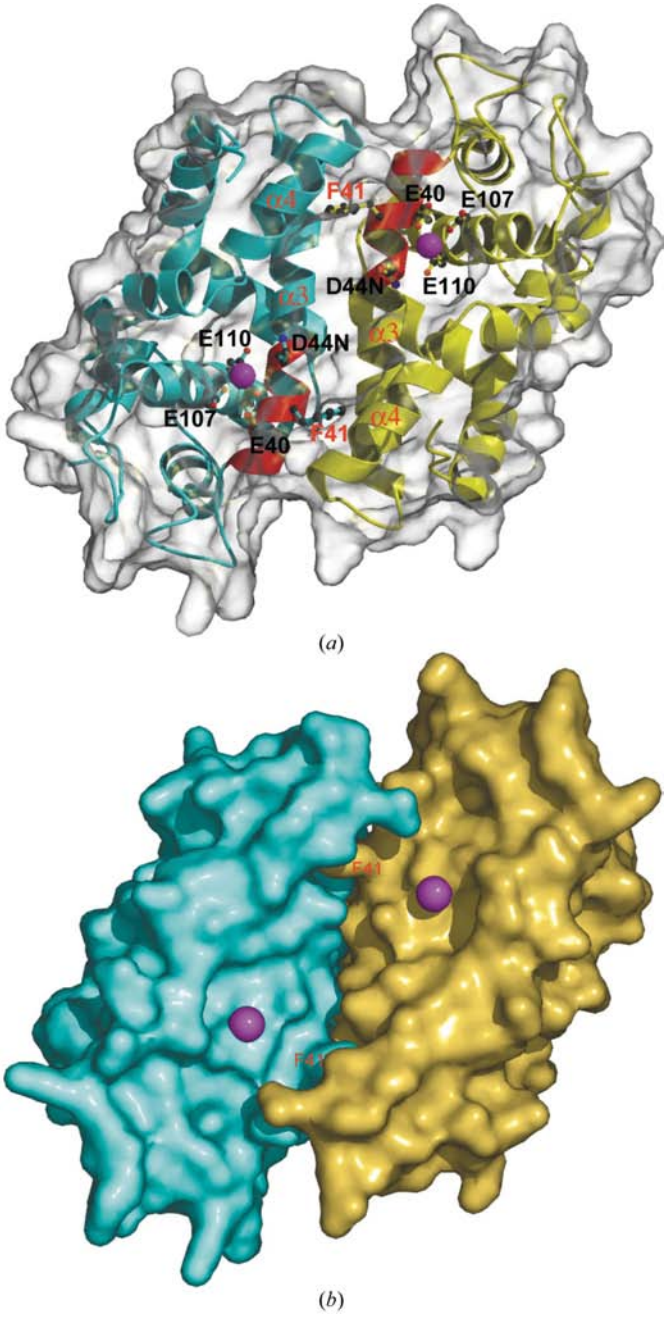

Figure 2
Surface representations of the endoND dimer (PDB codes 1jfz and 1rc5; Table 1). (*a*) The endoND dimer is outlined with transparent surfaces. The protein is illustrated as ribbon diagrams (helices as spirals, β-strands as arrows and loops as pipes) with the two subunits colored cyan and yellow, respectively. The signature motif at the N-terminus of α3 and the Mg^{2+} ions are highlighted in red and purple, respectively. The four acidic side chains and the side chain of Phe41 are shown as ball-and-stick models in an atomic colour scheme (carbon in black, nitrogen in blue and oxygen in red). (*b*) To highlight the subunit interface and the catalytic valley, the two endoNDs are outlined with nontransparent surfaces, one in cyan and the other in orange. The Mg^{2+} ions are shown as purple spheres and the two 'ball' (Phe41) side chains in the ball-and-socket junctions are indicated.

The dimerization of endoND creates a valley 50 Å long and 20 Å wide which can accommodate a dsRNA substrate and is therefore referred to as the catalytic valley (Fig. 2*b*). The two ball-and-socket junctions may be responsible in part for the accurate positioning of the two signature motifs in the catalytic valley and the protein fold locates residues Glu107 and Glu110, which are distant in the polypeptide chain, in proximity to the signature motif (Fig. 2*a*).

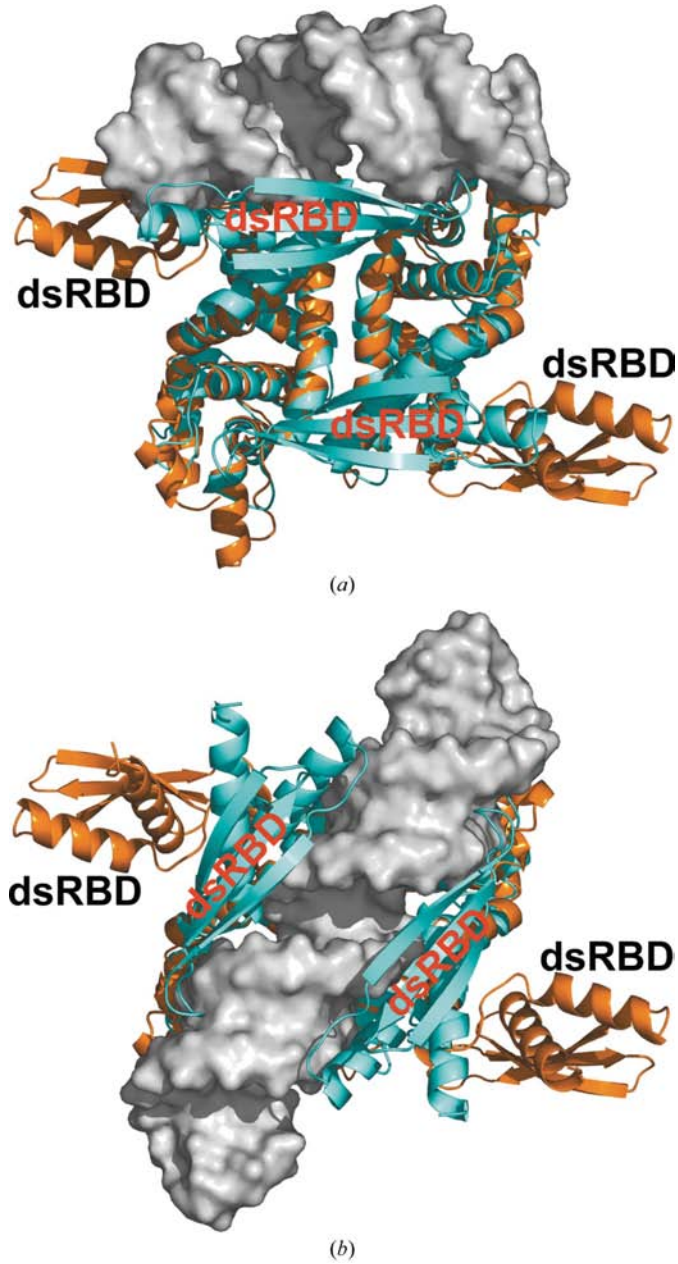

Figure 3
Induced fit. Schematic illustration of (*a*) the Aa-RNase III(E110K)–dsRNA structure (PDB code 1rc7; Table 1) and (*b*) the Aa-RNase III(D44N)–dsRNA structure (PDB code 2ez6) superimposed on the RNA-free Tm-RNase III structure (PDB code 1o0w) on the basis of C^{α} positions in the endoND dimer, showing a dramatic rotation and shift of dsRBD with respect to the endoND. The proteins are illustrated as ribbon diagrams (helices as spirals, β-strands as arrows and loops as pipes) and colored cyan for Aa-RNase III and orange for Tm-RNase III. The dsRNA is shown as a surface representation in gray.

A metal-ion-coordinated cluster of four acidic side chains, Glu40, Asp44, Asp107 and Glu110, was revealed by two endoND structures of Aa-RNase III with bound metal ions (PDB codes 1jfz and 1rc5; Table 1). The four side chains are conserved, among which Glu40 and Asp44 are located in the signature motif (Fig. 1*b*). In both Ec-RNase III and Dicer, residues Asp44 and Glu110 were proven to be essential for catalysis (Inada *et al.*, 1989; Li & Nicholson, 1996; Dasgupta *et al.*, 1998; Blaszczyk *et al.*, 2001; Sun & Nicholson, 2001; Sun *et al.*, 2004; Zhang *et al.*, 2004), whereas in the *E. coli* enzyme the impact of side chains Glu40 and Asp107 on catalysis is dependent on Mg^{2+} concentration (Sun *et al.*, 2004). The structure of Aa-RNase III(D44N) in complex with the product of dsRNA cleavage (PDB code 2ez6; Table 1) indicated that this metal-coordinated cluster of acidic side chains is indeed the RNA-cleavage site (Gan *et al.*, 2006). There are two RNA-cleavage sites in the catalytic valley (Fig. 2) and the distance between the two metal ions is 22.4 Å (Blaszczyk *et al.*, 2001; Gan *et al.*, 2006).

2.2. The dsRBD: induced fit upon dsRNA binding

The structural basis for the induced fit of RNase III is provided by the presence of a linker ($_{145}$EGRVKKD$_{151}$) between the endoND and the dsRBD. Because both the endoND and the dsRBD are relatively rigid, the flexibility of the linker is responsible for major conformational changes within the molecule (Gan *et al.*, 2005, 2006). In the six crystal structures of full-length Aa-RNase III in complex with dsRNA (PDB codes 1rc7, 1yyk, 1yyo, 1yyw, 1yy9 and 2ez6; Table 1), the relative orientations between the endoNDs and the dsRBDs vary dramatically (Blaszczyk *et al.*, 2004; Gan *et al.*, 2005, 2006). To date, the structure of *Thermotoga maritima* RNase III (Tm-RNase III; PDB code 1o0w; Table 1) is the only RNA-free structure of a full-length RNase III protein. Alignment of the Tm-RNase III structure with Aa-RNase III(E110K)–dsRNA (PDB code 1rc7; Fig. 3*a*) and with Aa-RNase III(D44N)–dsRNA (PDB code 2ez6; Fig. 3*b*) indicate a dramatic rotation and shift of the dsRBD with respect to the endoND dimer upon the binding of dsRNA.

The flexibility of the linker was further demonstrated by the structure of *Mycobacterium tuberculosis* endoND (Mt-endoND; PDB code 2a11; Table 1); although the full-length protein was crystallized, the dsRBD was totally disordered and therefore was not observed (Akey & Berger, 2005). In fact, before any structural information became available, genetic evidence indicated that the flexibility of the linker was important (Inada & Nakamura, 1995). It was also shown that the length of the linker may vary; extension of the linker from nine to 20 amino acids in Ec-RNase III does not affect cleavage-site selection (Conrad *et al.*, 2001). In Dicer, the linker between the second endoND and the dsRBD is ~15 residues in length (Fig. 1*a*). Therefore, a similar induced-fit event is expected for Dicer upon the recognition of a dsRNA substrate.

3. Structural basis for non-catalytic activity of RNase III

3.1. Catalytic antideterminants of RNase III

Catalytic antideterminants uncouple the RNA-binding and processing activities of RNase III. They can be either a special structural motif embedded in the RNA (Calin-Jageman *et al.*, 2001; Calin-Jageman & Nicholson, 2003) or a defective mutation in the protein (Inada & Nakamura, 1995; Blaszczyk *et al.*, 2004). In both cases, it is the interaction between the catalytic valley and the dsRNA that is disrupted.

3.2. A defective mutation as antideterminant

In Ec-RNase III, residue Gln153 is located in the middle of the flexible linker between the endoND and the dsRBD. The Q153P substitution in Ec-RNase III abolished RNA-cleavage activity but retained dsRNA-binding activity (Inada & Nakamura, 1995). This residue is not conserved; in Aa-RNase III the analogous residue is Lys149. It may be that the significance of the Ec-RNase III Q153P mutation resides in the mutational change to a Pro residue in the middle of the linker, which may reduce the flexibility of the segment. Thus, reorientation of the dsRBD–dsRNA structure after the initial binding of dsRNA by dsRBD may be inhibited in the mutant (Gan *et al.*, 2006). The structure of the Ec-RNase III(Q153P)–dsRNA complex remain to be determined.

As depicted in Fig. 3(*a*), the dsRNA in the Aa-RNase III(E110K)–dsRNA complex (PDB code 1rc7; Table 1) is not bound in the catalytic valley. Instead, the resulting dsRBD–dsRNA complex is perpendicular to the valley. As discovered previously (Blaszczyk *et al.*, 2004), Lys110 NZ essentially occludes the Mg^{2+}-binding site and forms a hydrogen-bond network involving Glu40, Asp44, Asp107 and two water molecules, rendering this environment in Aa-RNase III(E110K) no longer suitable for the binding of Mg^{2+}. Without the catalytically required Mg^{2+} ion, the protein cannot be functional in terms of RNA cleavage. It is also known that the divalent metal ion enhances dsRNA binding (Li & Nicholson, 1996; Sun & Nicholson, 2001). Without bound Mg^{2+}, the remaining negative charges in the catalytic valley are unfavorable for the binding of dsRNA, thereby giving rise to a distinct dsRNA-binding form in which the dsRNA is not bound within the valley and therefore cannot be processed (Fig. 3*a*). Thus, the E110K mutation acts as a catalytic antideterminant of RNase III, uncoupling the dsRNA-binding and processing abilities of the enzyme (Blaszczyk *et al.*, 2004).

Other known mutations of RNase III that completely uncouple dsRNA binding and processing include E110Q (Sun & Nicholson, 2001) and E110A (Li & Nicholson, 1996). The structures of these mutants in complex with dsRNA remain to be determined. Therefore, how these two mutations uncouple the RNA binding and processing is not clear.

3.3. A special structural motif in dsRNA as antideterminant

The positive expression of CIII and Int in bacteriophage λ are two examples where genetic control may be exerted by

site-specific dsRNA binding of RNase III in the absence of processing (Guarneros, 1988; Oppenheim *et al.*, 1993). In these two special cases, the endoND may still be functional but the respective CIII and Int mRNA may not be bound in the catalytic valley. A special structural motif in the RNA of these two genes might act as an antideterminant for dsRNA processing, which remains to be seen. The first direct evidence of RNA-structure-dependent uncoupling of substrate recognition and cleavage by the wild-type Ec-RNase III was the R1.1[CL3B] RNA, a dsRNA mutant derived from the T7 phage R1.1 RNase III substrate and selected to be resistant to cleavage *in vitro* but to retain binding affinity (Calin-Jageman & Nicholson, 2003). This mutant RNA contains a special bulge–helix–bulge motif that may act as an antideterminant for catalytic processing. In light of the structure of Aa-RNase III(E110K)–dsRNA (PDB code 1rc7; Table 1), the bulge–helix–bulge motif in R1.1[CL3B] may act by blocking the binding of dsRNA in the catalytic valley. Therefore, the catalytic antideterminants embedded in the dsRNA may be anti-endoND but not anti-dsRBD, which may also be the case in ethidium-dependent uncoupling of substrate binding and cleavage by Ec-RNase III (Calin-Jageman *et al.*, 2001), in which two ethidium-binding sites exist in the R1.1 RNA and the site-specific binding of ethidium to the RNA substrate perturbs substrate recognition by the endoND. It is not clear how the special structures in the RNAs uncouple the binding and cleavage because the structures of RNase III in complex with these RNAs are not available.

4. Structural insight into the mechanism of dsRNA processing by RNase III

4.1. RNA-cleavage site in the product complex of Aa-RNase III(D44N)

The RNase III-catalyzed dsRNA processing is Mg^{2+}-ion-dependent and probably proceeds in a single step *via* an S_N2 (bimolecular nucleophilic substitution) type mechanism (Robertson *et al.*, 1968; Dunn, 1982; Li & Nicholson, 1996; Sun & Nicholson, 2001; Campbell *et al.*, 2002). The Aa-RNase III(D44N)–dsRNA structure (PDB code 2ez6; Table 1), containing the product of dsRNA cleavage, reveals that each RNA-cleavage site is composed of amino-acid residues Glu40, Asp44, Asp107 and Glu110 from one subunit, nucleotide residues R−1, R0 and R+1, the Mg^{2+} ion and three water molecules (Fig. 4). The Mg^{2+} ion coordinates with three acidic side chains (Asp40, Asp107 and Glu110) and the three water molecules (1, 2 and 3), assuming the geometry of an octahedron. In addition to interacting with the metal ion, Glu110 is also hydrogen bonded to water 2 which, together with water 1, interacts with the 5′-phosphate of the RNA (Fig. 4). The coordination of Mg^{2+} in the product complex is slightly different from that in the RNA-free structures (Gan *et al.*, 2006). All components of the metal-ion coordination adjust slightly upon RNA binding. Comparatively, the Mg^{2+} octahedron in the product complex is more distorted. Water molecule 2 always bridges the interaction between the metal ion and the Asp44 side chain, whereas water 3 is hydrogen bonded to the Glu110 side chain only in the RNA-free state (Fig. 4). Least affected upon RNA binding are the side chains of Glu40 and Asp107, which are not located in proximity to the scissile bond, in agreement with the previously proposed roles of these two residues in metal binding (Sun *et al.*, 2004). However, there is a stringent functional requirement for both the charge and size of the Asp44 and Glu110 side chains which, together with their locations and their relationship with other components of the cleavage site, indicates the involvement of a second metal ion in the mechanism of scissile-bond cleavage.

4.2. Two-metal-ion catalysis

RNase III enzymes belong to a superfamily of polynucleotidyl transferases that includes RNases, DNases and transposases. Two-metal-ion catalysis has been established for both Tn5 transposase (Davies *et al.*, 2000; Steiniger-White *et al.*, 2004) and RNase H (Nowotny *et al.*, 2005) and has been suggested for RNase III (Sun *et al.*, 2005). Tn5 transposase is specific for DNAs and no water is involved in catalysis, while RNase H is specific for RNA–DNA heteroduplexes and two water molecules are involved in catalysis (Nowotny *et al.*, 2005). Although RNase H is specific for RNA/DNA hybrids while RNase III is specific for dsRNA, the catalytic events for the two enzymes are the same, *i.e.* metal-dependent and sequence-nonspecific hydrolysis of an RNA phosphodiester bond.

To date, four crystal structures of bacterial RNase III in complex with metal ions have been reported, including Aa-endoND–Mn^{2+}, Aa-endoND–Mg^{2+}, Mt-endoND–Ca^{2+} and Aa-RNase III(D44N)–dsRNA–Mg^{2+} (PDB codes 1jfz, 1rc5, 2a11 and 2ez6; Table 1). In all three structures of Aa-RNase III (PDB codes 1jfz, 1rc5 and 2ez6), only one metal ion (either Mn^{2+} or Mg^{2+}) was observed per polypeptide chain (Fig. 4), which is referred to as metal site 1 (Fig. 5). In the Mt-endoND–Ca^{2+} structure (PDB code 2a11), two metal ions were identified per subunit; the locations of the two Ca^{2+} ions in the two subunits are virtually identical (Akey & Berger, 2005). One of the two Ca^{2+} ions is located near metal site 1 as identified in the Aa-RNase III structures, whereas the other is located between the side chains of Glu40 and Asp107 and the phosphate bridge between R0 and R+1, which is referred to as metal site 2 (Fig. 5). Recently, a 3.3 Å structure of *Giardia intestinalis* (Gi) Dicer was reported (PDB code 2ffl; MacRae *et al.*, 2006) in which two Mn^{2+} ions were found close to the cleavage site in each endoND. One of the two Mn^{2+} ions occupies metal site 1, but the second Mn^{2+} ion occupies different positions in the two endoNDs. In one endoND, the second Mn^{2+} ion occupies metal site 2, whereas in the other it is located between the side chains of Asp44 and Glu110 near the scissile bond, which is referred to as metal site 3 (Fig. 5).

Metal ion 1 is a catalytic cation. In Aa-RNase III(D44N)–dsRNA–Mg^{2+} (PDB code 2ez6; Table 1), this metal ion coordinates with three acidic side chains (GluE40, Asp107 and Glu110) and three water molecules (1, 2 and 3), assuming the

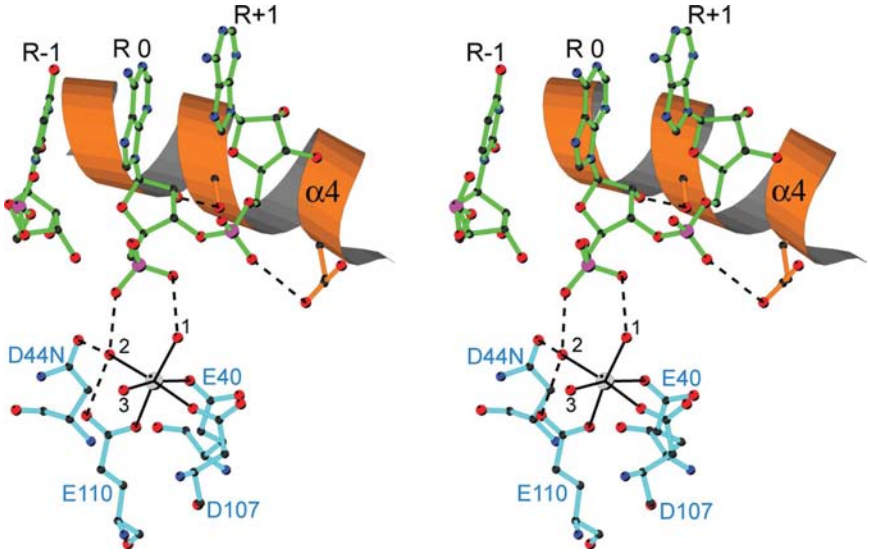

Figure 4
Cleavage-site structure in the product complex of Aa-RNase III. Stereoview showing the cleavage-site architecture observed in the Aa-RNase III(D44N)–dsRNA structure (PDB code 2ez6; Table 1). Residues are shown as ball-and-stick models in an atomic color scheme (carbon in black, nitrogen in blue, oxygen in red, phosphorous in purple and magnesium in gray). The nucleotide residue in the cleavage site is numbered R0 and the others are numbered according to the polarity of the RNA strand. The α4 helix from the partner subunit is shown as a ribbon diagram. Metal-coordination bonds are illustrated as solid lines, with hydrogen bonds as dashed lines. The two endoND subunits and the RNA are indicated in cyan and orange and in green, respectively.

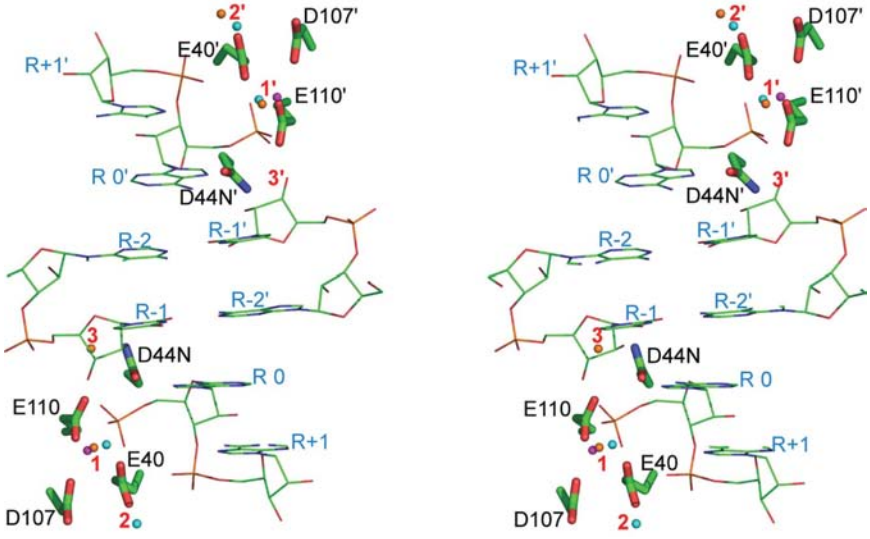

Figure 5
Metal ions identified in the cleavage site of RNase III structures. Stereoview showing the superposition of the metal ions (Mg^{2+}, Ca^{2+} and Mn^{2+}) found in the RNA-cleavage sites of Aa-RNase III(D44N)–dsRNA–Mg^{2+} (PDB code 2ez6; Table 1), Mt-endoND–Ca^{2+} (PDB code 2a11) and Gi-Dicer–Mn^{2+} (PDB code 2ffl; MacRae *et al.*, 2006). For clarity, the cleavage-site residues of the Mt-endoND–Ca^{2+} and Gi-Dicer–Mn^{2+} structures are not shown. Amino-acid and nucleotide residues are shown as stick models in an atomic color scheme (carbon in green, nitrogen in blue, oxygen in red and phosphorus in orange). The nucleotide residues in the cleavage sites are numbered R0 and the others are numbered according to the polarity of the RNA strand. Metal ions, numbered in red, are shown as spheres in purple, cyan and orange for Mg^{2+}, Ca^{2+}, and Mn^{2+}, respectively. The two cleavage sites are distinguished by a prime in their labels.

geometry of an octahedron (Fig. 4). In addition to interacting with the metal ion, Glu110 is also hydrogen bonded to water 2 which, together with water 1, interacts with the 5′-phosphate created by the cleavage of the scissile bond (Fig. 4). Metal ion 2 is involved in RNA binding. In both Mt-endoND–Ca^{2+} (PDB code 2a11) and Gi-Dicer–Mn^{2+} (PDB code 2ffl), it is located near side chains Glu40 and Asp107 and the RNA-phosphate bridge between nucleotide residues R0 and R+1 (Fig. 5). Metal site 3 is a candidate for a second catalytic metal in the mechanism of proposed two-metal-ion catalysis. As revealed in the Gi-Dicer–Mn^{2+} structure (PDB code 2ffl), it is located near the Asp44 and Glu110 side chains and is ∼4.2 Å from metal ion 1 (MacRae *et al.*, 2006). In light of the Aa-RNase III(D44N)–dsRNA–Mg^{2+} structure (PDB code 2ez6), metal ion 3 is most likely to be the second catalytic ion because it is in proximity to the scissile bond (Fig. 5). The catalytic valley of RNase III is highly negatively charged (Blaszczyk *et al.*, 2001); additional metal ions may be involved in the binding of dsRNA.

4.3. Characteristic two nucleotide 3′-overhang of RNase III products

The crystal structure of the RNase III–product complex (PDB code 2ez6; Table 1) indicates that the hydrolysis of the scissile bond is carried out by metal-coordinated side chains of Glu40, Asp44, Asp107 and Glu110 (Fig. 4), that two RNA-cleavage sites are located in the catalytic valley of the endoND dimer (Fig. 2), that a single RNA-cleavage event occurs on each strand of the RNA within each cleavage site, resulting in a terminal phosphate group at the 5′-end of each strand, and that the two RNA-cleavage events together create two-nucleotide (nt) 3′-overhangs (Fig. 6). The 3′-hydroxyl and 5′-phosphate groups and the 2 nt 3′-overhang are hallmarks of RNase III reaction products. It has been implicated that the 5′-phosphate groups of each strand are essential for the incorporation of siRNAs into the RNAi pathway (Schwarz *et al.*, 2002). It has also been shown that short RNA duplexes without the 2 nt 3′-overhang do not initiate RNA interference (Ohmichi *et al.*, 2002). Intriguingly, the structure of the product complex (PDB code 2ez6; Table 1) also indicates that the metal-coordinated

acidic side chains Glu40, Asp44, Asp107 and Glu110 of one subunit cannot function alone without the participation of partner subunit because, as shown in Fig. 4, residues in the α4 helix from the partner subunit are involved in substrate recognition and scissile-bond selection (Gan *et al.*, 2006). Therefore, endoND dimerization is essential for the RNA-processing activity of RNase III family members.

5. Conclusions

Bacterial RNase III affects post-transcriptional gene expression by two different mechanisms through two distinct forms of protein–dsRNA complex. Induced fit, facilitated by a flexible linker between the endoND and the dsRBD, occurs during protein–RNA recognition (Fig. 3). While the Aa-RNase III(E110K)–dsRNA structure (PDB code 1rc7) represents a non-catalytic ensemble, the Aa-RNase III(D44N)–dsRNA structure (PDB code 2ez6) is the first catalytic complex. The information about the mechanism of RNA hydrolysis can be extrapolated to other members of the RNase III family.

The dimerization of endoND is essential for dsRNA processing because it (i) creates the catalytic valley (Fig. 2*b*) for the binding of a dsRNA substrate and (ii) precisely positions the two RNA-cleavage sites with respect to the two RNA strands of a bound substrate for the creation of a characteristic 2 nt 3′-overhang of RNase III product with 3′-OH and 5′-phosphate ends (Figs. 5 and 6). For the hydrolysis of each RNA strand, metal-coordinated side chains from one endoND carry out the cleavage chemistry, while side chains from the partner subunit are involved in substrate recognition and scissile-bond selection (Fig. 4). The available structural and biochemical data suggest the requirement as well as the location of a second divalent cation in the hydrolysis of each of the two RNA strands. It is ∼4.0 Å away from metal ion 1, in proximity to the scissile bond between nucleotide residues R0 and R−1, and interacts with the strictly conserved amino-acid side chains Asp44 and Glu110 (Fig. 5). Additional structural information is needed for a complete mechanism of dsRNA processing by RNase III enzymes.

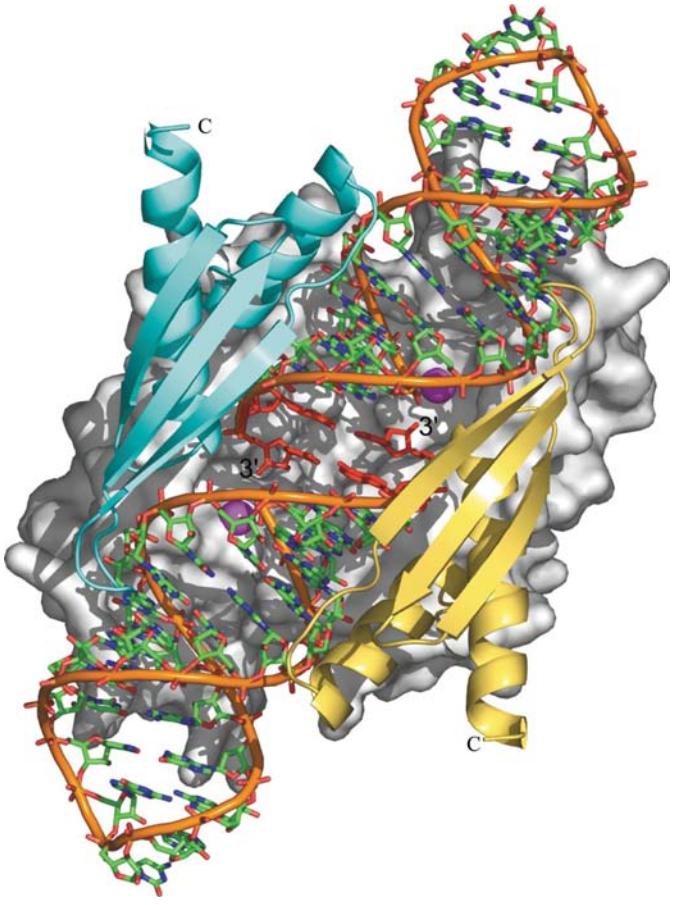

Figure 6
The product complex of Aa-RNase III, a symmetric dsRNA-dicing machine. The endoND dimer in the structure of Aa-RNase III(D44N)–dsRNA–Mg^{2+}) (PDB code 2ez6; Table 1) is outlined with a molecular surface. The two dsRBDs are illustrated as ribbon diagrams (helices as spirals, β-strands as arrows and loops as pipes) and colored in cyan and yellow, respectively. The Mg^{2+} ions are shown as purple spheres. The product molecules are illustrated as stick models with highlighted backbones in orange. An atomic color scheme (carbon in green, nitrogen in blue, oxygen in red and phosphorus in orange) is used for the RNA, except for the 2 nt 3′-overhangs, which are highlighted in red.

I would like to thank all my coworkers who contributed to the work cited from this laboratory. I am particularly indebted to Drs Jaroslaw Blaszczyk, Jianhua Gan and Joseph Tropea for their invaluable contributions. This research was supported by the Intramural Research Program of the NIH, National Cancer Institute, Center for Cancer Research.

References

Akey, D. L. & Berger, J. M. (2005). *Protein Sci.* **14**, 2744–2750.
Amarasinghe, A. K., Calin-Jageman, I., Harmouch, A., Sun, W. & Nicholson, A. W. (2001). *Methods Enzymol.* **342**, 143–158.
Bernstein, E., Caudy, A. A., Hammond, S. M. & Hannon, G. J. (2001). *Nature (London)*, **409**, 363–366.
Blaszczyk, J., Gan, J., Tropea, J. E., Court, D. L., Waugh, D. S. & Ji, X. (2004). *Structure*, **12**, 457–466.
Blaszczyk, J., Tropea, J. E., Bubunenko, M., Routzahn, K. M., Waugh, D. S., Court, D. L. & Ji, X. (2001). *Structure*, **9**, 1225–1236.
Calin-Jageman, I., Amarasinghe, A. K. & Nicholson, A. W. (2001). *Nucleic Acids Res.* **29**, 1915–1925.
Calin-Jageman, I. & Nicholson, A. W. (2003). *Nucleic Acids Res.* **31**, 2381–2392.
Campbell, F. E. Jr, Cassano, A. G., Anderson, V. E. & Harris, M. E. (2002). *J. Mol. Biol.* **317**, 21–40.
Carthew, R. W. (2001). *Curr. Opin. Cell Biol.* **13**, 244–248.
Conrad, C., Evguenieva-Hackenberg, E. & Klug, G. (2001). *FEBS Lett.* **509**, 53–58.
Court, D. (1993). *RNA Processing and Degradation by RNase III*, edited by J. G. Belasco & G. Braverman, pp. 71–116. New York: Academic Press.
Dasgupta, S., Fernandez, L., Kameyama, L., Inada, T., Nakamura, Y., Pappas, A. & Court, D. L. (1998). *Mol. Microbiol.* **28**, 629–640.
Davies, D. R., Goryshin, I. Y., Reznikoff, W. S. & Rayment, I. (2000). *Science*, **289**, 77–85.
Dunn, J. J. (1976). *J. Biol. Chem.* **251**, 3807–3814.
Dunn, J. J. (1982). *Ribonuclease III*, edited by P. Boyer, pp. 485–499. New York: Academic Press.
Filippov, V., Solovyev, V., Filippova, M. & Gill, S. S. (2000). *Gene*, **245**, 213–221.

Gan, J., Tropea, J. E., Austin, B. P., Court, D. L., Waugh, D. S. & Ji, X. (2005). *Structure*, **13**, 1435–1442.
Gan, J., Tropea, J. E., Austin, B. P., Court, D. L., Waugh, D. S. & Ji, X. (2006). *Cell*, **124**, 355–366.
Guarneros, G. (1988). *Curr. Top. Microbiol. Immunol.* **136**, 1–19.
Inada, T., Kawakami, K., Chen, S. M., Takiff, H. E., Court, D. L. & Nakamura, Y. (1989). *J. Bacteriol.* **171**, 5017–5024.
Inada, T. & Nakamura, Y. (1995). *Biochimie*, **77**, 294–302.
Kameyama, L., Fernandez, L., Court, D. L. & Guarneros, G. (1991). *Mol. Microbiol.* **5**, 2953–2963.
Kharrat, A., Macias, M. J., Gibson, T. J., Nilges, M. & Pastore, A. (1995). *EMBO J.* **14**, 3572–3584.
Krainer, A. (1997). *Eukaryotic mRNA Processing.* New York: IRL Press.
Li, H., Chelladurai, B. S., Zhang, K. & Nicholson, A. W. (1993). *Nucleic Acids Res.* **21**, 1919–1925.
Li, H. & Nicholson, A. W. (1996). *EMBO J.* **15**, 1421–1433.
MacRae, I. J., Zhou, K., Li, F., Repic, A., Brooks, A. N., Cande, W. Z., Adams, P. D. & Doudna, J. A. (2006). *Science*, **311**, 195–198.
Nicholson, A. W. (1996). *Prog. Nucleic Acid Res. Mol. Biol.* **52**, 1–65.
Nicholson, A. W. (1999). *FEMS Microbiol. Rev.* **23**, 371–390.
Nicholson, A. W. (2003). *The Ribonuclease Superfamily: Forms and Functions in RNA Maturation, Decay and Gene Silencing*, edited by G. J. Hannon, pp. 149–174. Cold Spring Harbor, New York: Cold Spring Harbor Laboratory Press.
Nowotny, M., Gaidamakov, S. A., Crouch, R. J. & Yang, W. (2005). *Cell*, **121**, 1005–1016.
Ohmichi, T., Karimata, H. & Sugimoto, N. (2002). *Nucleic Acids Res. Suppl.*, pp. 63–64.
Oppenheim, A. B., Kornitzer, D., Altuvia, S. & Court, D. L. (1993). *Prog. Nucleic Acid Res. Mol. Biol.* **46**, 37–49.
Robertson, H. D. (1982). *Cell*, **30**, 669–672.
Robertson, H. D. & Dunn, J. J. (1975). *J. Biol. Chem.* **250**, 3050–3056.
Robertson, H. D., Webster, R. E. & Zinder, N. D. (1968). *J. Biol. Chem.* **243**, 82–91.
Schwarz, D. S., Hutvagner, G., Haley, B. & Zamore, P. D. (2002). *Mol. Cell*, **10**, 537–548.
Steiniger-White, M., Rayment, I. & Reznikoff, W. S. (2004). *Curr. Opin. Struct. Biol.* **14**, 50–57.
Sun, W., Li, G. & Nicholson, A. W. (2004). *Biochemistry*, **43**, 13054–13062.
Sun, W. & Nicholson, A. W. (2001). *Biochemistry*, **40**, 5102–5110.
Sun, W., Pertzev, A. & Nicholson, A. W. (2005). *Nucleic Acids Res.* **33**, 807–815.
Wu, H., Xu, H., Miraglia, L. J. & Crooke, S. T. (2000). *J. Biol. Chem.* **275**, 36957–36965.
Zhang, H., Kolb, F. A., Jaskiewicz, L., Westhof, E. & Filipowicz, W. (2004). *Cell*, **118**, 57–68.